Chapter 7

The annealing mechanism of AuGe/Ni/Au ohmic contacts to a two-dimensional electron gas

Ohmic contacts to a two-dimensional electron gas (2DEG) in GaAs heterostructures are often realized by annealing of AuGe/Ni/Au that is deposited on its surface. We studied how the quality of this type of ohmic contact depends on the annealing time and temperature, and how these parameters depend on the depth of the 2DEG below the surface. Combined with transmission electron microscopy and energy-dispersive X-ray spectrometry studies of the annealed contacts, our results allow for identifying the annealing mechanism and describing a model that can predict optimal annealing parameters for a certain heterostructure.

This chapter is based on Ref. 3 on p. 131.

7.1 Introduction

Epitaxially grown GaAs/AlGaAs heterostructures that contain a two-dimensional electron gas (2DEG) are widely used for electron transport studies in low-dimensional systems [1]. Establishing electrical contacts to the 2DEG is a crucial step in device fabrication with these heterostructures. A commonly used recipe for making ohmic contacts is annealing of a AuGe/Ni/Au alloy that has been deposited on the heterostructure surface [2]. High-quality heterostructures are often only available in a limited quantity, and it is desirable to minimize the heating that is needed for annealing the contacts to avoid damaging the heterostructure. A model that predicts optimal annealing times and temperatures for a heterostructure with the 2DEG at a certain depth is therefore very valuable.

We present here a study of the annealing mechanism for this type of ohmic contact, and a model that can predict optimal annealing parameters for a certain heterostructure. We used electron transport experiments to study how the quality of AuGe/Ni/Au based ohmic contacts depends on annealing time and temperature, and how these parameters change with the depth of the 2DEG below the surface. These results confirm that the annealing mechanism cannot be described by a single simple diffusion process. Cross-sectional studies of annealed contacts with Transmission Electron Microscope (TEM) and Energy Dispersive X-ray (EDX) techniques were used for identifying a more complex annealing mechanism, that is in agreement with the results from our electron transport studies.

The AuGe/Ni/Au contact was first introduced by Braslau *et al.* [3] to contact n-GaAs, and several studies aimed at understanding the contact mechanism for this type of contact [4, 5, 6, 7, 8, 9]. Later studies focussed on the formation of an ohmic contact to a 2DEG in a GaAs/AlGaAs heterostructure [10, 11, 12], but do not report how the optimal annealing parameters depend on the depth of the 2DEG below the surface. A number of these studies suggest that a contact is formed because a pattern of Au/Ni/Ge spikes that originate from the metallization penetrate the heterostructure, just beyond the depth of the 2DEG. We observe, instead, a mechanism where metal-rich phases only penetrate the heterostructure over a distance that is shorter than the depth of the 2DEG. The mechanism that results in a good contact is then similar to a process that has been described [5] for contacts to n-GaAs: during annealing, the AuGe/Ni/Au on the surface segregates in Ni and Au domains, where the Ni domains contain most of the Ge. These domains penetrate the heterostructure and grow towards the

2DEG in large grains rather than narrow spikes. For optimal electrical contact conditions the Au and Ni grains do not reach the 2DEG. The contact resistance decreases and the contact becomes ohmic because Ge diffuses deeper, forming a highly doped AlGaAs region between the 2DEG layer and metal-rich phases at the surface [3]. Recently Sai Saravanan *et al.* found that also Ni and Au diffuse deeper into the heterostructure in comparable concentrations as Ge [12]. Nevertheless, we find that even for very long annealing times, when the contact resistance has significantly increased compared to the optimal contact, the Au and Ni-rich phases still do not penetrate the 2DEG.

7.2 Fabrication

We studied annealed AuGe/Ni/Au contacts to three GaAs/AlGaAs heterostructures with the 2DEG at a heterojunction at 70 nm (wafer A), 114 nm (wafer B), and 180 nm (wafer C) below the surface of the wafer. These wafers have similar values for the 2DEG electron density n_s and mobility μ (around $2 \cdot 10^{15}\,\mathrm{m}^{-2}$ and $100\mathrm{m}^2/\mathrm{Vs}$, respectively, results for 4.2 K and samples kept in the dark during cool down). For all three wafers the layer structure (from the surface down) is very similar besides the depth of the 2DEG. The top layer is a ~ 5 nm n-GaAs capping layer, then a $\mathrm{Al}_y\mathrm{Ga}_{1-y}\mathrm{As}$ doping layer (Si at $\sim 1 \cdot 10^{18}\,\mathrm{cm}^{-3}$) with $y \approx 0.32$, of thickness 30 nm (B), 72 nm (B) or 140 nm (C). After this follows an undoped $\mathrm{Al}_y\mathrm{Ga}_{1-y}\mathrm{As}$ buffer layer (~ 35 nm thick). The 2DEG is located at the interface with the next layer, which is a thick undoped GaAs layer.

We studied 200 x 200 $\mu\mathrm{m}^2$ contacts that were defined by optical lithography on a 1 mm wide and 2 mm long etched mesa. An electron-beam evaporator was used for deposition of subsequently 150 nm AuGe of eutectic composition (12 wt% Ge), 30 nm of Ni and 20 nm of Au. Subsequent annealing took place in a pre-heated quartz furnace tube in a N_2 flow to prevent oxidation. We have used three different annealing temperatures, 400 °C, 450 °C and 500 °C (all higher than the AuGe eutectic melting temperature of °C). The samples were placed on a quartz boat and then moved into the center of the oven for a various annealing times. Figure 7.1a shows the temperature of the surface of the quartz boat as a function of time for an oven temperature of 450 °C. We assume that the sample temperature closely follows the temperature of the quartz boat, since we assured a good thermal contact over the full surface of the sample.

We measured the current-voltage (IV) characteristics of all contacts to determine optimal annealing parameters. We found that a suitable and sufficient

definition for an optimal ohmic contact is a contact with the lowest zero-bias resistance at 4.2 K. The typical resistance for such a contact is $\sim 20\ \Omega$, but we have observed resistances as low as 5 Ω. All contacts defined as optimal in this manner showed highly linear IVs up to at least 1 mV (over and under annealed contacts did show non-linear IVs due to effects like Schottky or tunnel barriers in the contacts). Further, all these optimal contacts showed a strong monotonous reduction of the contact resistance upon lowering the sample temperature from 300 K to 4.2 K. Highly over and under annealed contacts showed an increase of the contact resistance upon cooling to 4.2 K.

7.3 Electrical measurements

We used a current-biased 4-terminal configuration to measure the voltage drop across a single contact, with two terminals attached to the metal bond wire to the ohmic contact, and two others attached via the 2DEG (this allowed us to use a standard sample design in our fabrication facility). We are aware that the Transmission Line Method (TLM) [13] is a better method for determining the exact value of a contact resistance, but this is not needed for our approach. We compare resistances of various annealed contacts that were fabricated under identical conditions besides the variation in annealing time and temperature. Within such a set, we determine which contacts have the lowest contact resistance. When reproducing our results with contacts that were fabricated in a different batch (using the same electron-beam evaporator, but after replenishing the AuGe target), we find that the values of the lowest contact resistance can be different up to a factor 2 around the typical result. We attribute these batch-to-batch fluctuations to variations in the exact composition of the AuGe/Ni/Au layer that we deposit. The optimal annealing times, however, show batch-to-batch fluctuations of only 10%. Thus, our approach for determining optimal annealing conditions does not depend on the absolute value of the contact resistance.

Figure 7.1b shows a typical result, from which we determine the optimal annealing time for contacts to wafer C for the case of annealing with the oven at 450 °C. Contact resistance data that is denoted as $\langle R \rangle$ is the average resistance measured on a set of 8 identical contacts, the error bar is an indication for the standard deviation. The results in Fig. 7.1b show a clear minimum in contact resistance for annealing times near 5 minutes. We fit a parabola (phenomenological ansatz) to the $\log\langle R \rangle$ values of these data points, and define the optimal annealing time as the time coordinate of the minimum of the parabola. In this

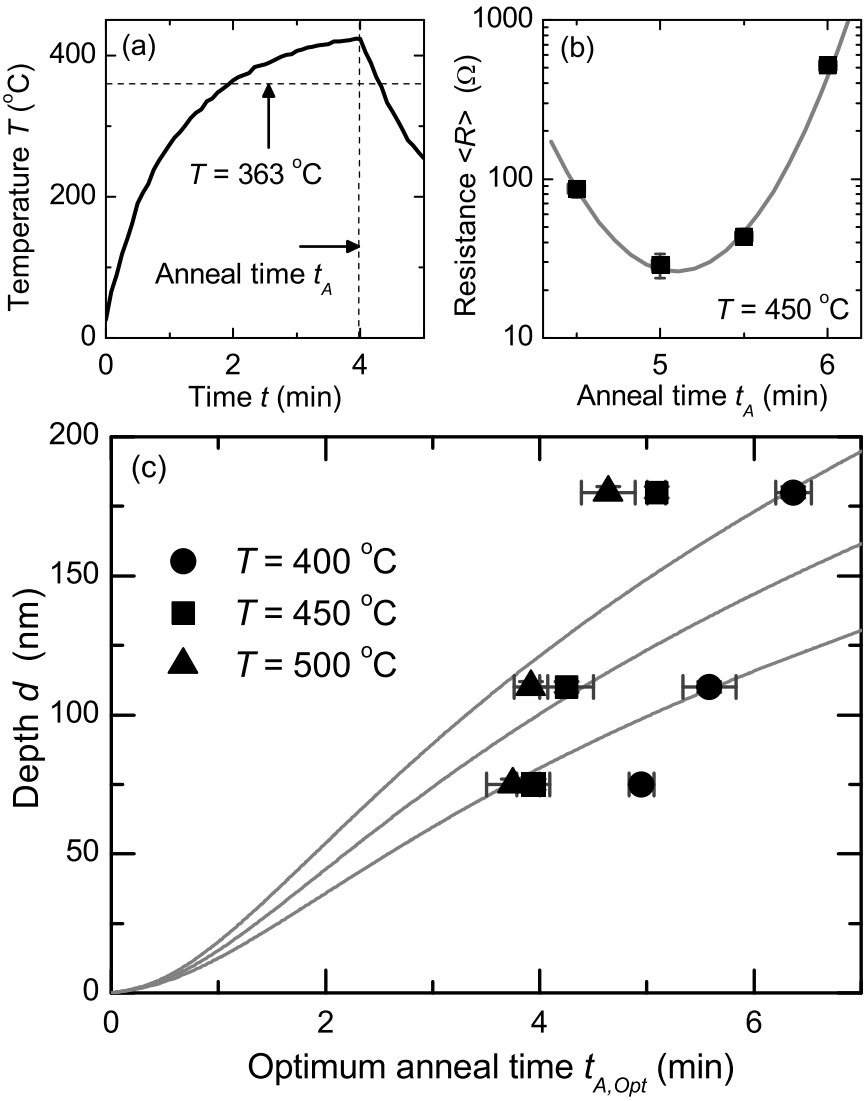

Figure 7.1: **(a)** Temperature of the quartz boat as a function of time for an oven temperature of 450 °C. Horizontal dashed line indicates the AuGe melting temperature $T = 363$ °C. The vertical dashed line indicates our definition of the annealing time t_A, the time at which the boat is taken out of the oven. **(b)** Average contact resistance $\langle R \rangle$ as a function of annealing time t_A for contacts on wafer C, annealed at 450 °C. A parabolic fit is made to estimate the annealing time where the resistance has a minimum. **(c)** Overview of optimal annealing times $t_{A,Opt}$ as a function of depth d of the 2DEG beneath the wafer surface for $T = 400$, 450 and 500 °C. The three gray lines (bottom to top for 400, 450 and 500 °C) are results of fitting a simple diffusion model to the experimental data (see text), which does not yield good fits.

manner, the optimal annealing times $t_{A,Opt}$ are obtained for contacts on wafers A, B and C, annealed at each of the temperatures.

Figure 7.1c presents these optimal annealing times. As expected, the optimal annealing time increases as the temperature is decreased, and increases as the depth d of the 2DEG increases. While it is known that several simultaneous diffusion processes play a role in contact formation [5], we will, for the sake of argument, show that a simple diffusion model has little value for predicting how optimal annealing times depend on the depth d and the annealing temperature. For this simple diffusion model, we assume that a certain dopant (with fixed concentration C_0 at the surface) diffuses into the heterostructure. The relevant solution to Fick's second law is then

$$C = C_0 \; erfc\frac{x}{\sqrt{4Dt}}. \tag{7.1}$$

Here C is the doping concentration at time t and depth x into the heterostructure, and D is the diffusion constant ($erfc$ is complementary error function). Since the temperature of our sample is not constant (see Fig. 7.1a) we will use the measured temperature profile $T(t)$ to integrate the diffusion constant over time, and use in Eq. 7.1 $\int D(t)dt$ instead of Dt, where

$$D(t) = D_0 \; exp(-\frac{E_a}{k_B T(t)}), \tag{7.2}$$

where E_a is an activation energy. We assume that an optimal contact then always occurs for a certain value for C/C_0 at the depth of the 2DEG ($x = d$). We define the annealing time as the time from start to the moment when the boat is taken out of the oven, but integrate over the entire time span that the sample is at elevated temperatures, (as shown in Fig. 7.1a, fully including the cooling down). This gives a model with the activation energy E_a, diffusion constant D_0 and concentration C/C_0 as fitting parameters.

The gray lines Fig. 7.1c shows the best fitting result that reasonably covers all 9 data points in a single fit. Besides the fact that the shape of the traces only poorly matches the trend in the data, the parameter values give unreasonable results. The temperature dependence alone governs the fitting result for E_a, giving here 0.15 eV. This is on the low side for typical values for diffusion in GaAs materials ($\sim$ 1 eV) [7]. For fixed E_a, various combinations of C/C_0 and D_0 give identical results. When assuming a typical value $D_0 \sim 3 \cdot 10^{-7}$ m^2/s (for diffusion of Au in GaAs [7]), this fit yields C/C_0 very close to 1, i.e. completely saturated diffusion. This is in contradiction with the clear dependence on depth

that we observe (and this remains the case when allowing for E_a up to ~ 1 eV, but then the fit does not cover all 9 data points at all). Thus, we find that predicting optimal annealing times with simple diffusion (according to $t_{A,Opt} \propto d^2$ at fixed temperature) does not work and that a more complex model needs to be considered.

7.4 Cross-sectional TEM imaging

We have studied the contact formation using cross-sectional TEM imaging of contacts at several stages during the annealing process. The samples were prepared for TEM imaging by using a Focussed Ion Beam (FIB) to slice out a micrometer thin piece of the measured contact. By further thinning using the FIB, the thickness was reduced to 100 nm.

Figure 7.2a shows an overview of an optimally annealed contact on wafer C which was annealed for 5 minutes at 450 °C. The composition of the various phases has been determined by Energy Dispersive X-ray (EDX) analysis and is illustrated in Fig. 7.2b. From bottom to top we recognize the GaAs substrate, and an AlAs/GaAs superlattice to smoothen the surface of the substrate. On top of that we find another layer of epitaxially grown GaAs and a layer of AlGaAs. The 2DEG is at the interface of these two layers. The GaAs capping layer that was originally on top of the AlGaAs layer is no longer visible. Instead we see large grains of Au and Ni that have penetrated below the original wafer surface. Both of these phases contain some out-diffused Ga and As, and the Ni forms a new phase absorbing most of the Ge. We find that the Au grains do not contain any Ge, consistent with the findings of Kuan *et al.* [5]. The wide and curved dark lines going over all the heterostructure layers (most clearly visible in the GaAs layers) are due to strain induced by the FIB sample preparation and are not related to the diffusion process.

We find that the Au and Ni grains do not have to penetrate the 2DEG in order to establish a good electrical contact. We can rule out that we do not see grains reaching the 2DEG due to the small thickness of the sample slice, since we observed no substantial variation in the penetration depth of a large number of Au and Ni grains going along the sample slice. We examined two slices from two different samples, both with a length of 100 μm, after electrical measurements confirmed that these contacts were indeed optimally annealed.

The TEM image in Fig. 7.2c shows a larger region of an optimally annealed contact. Large Au and Ni grains that have penetrated the AlGaAs layer can

be identified. Figure 7.2d shows an over annealed contact on wafer C, that was annealed for 7 minutes at 450 °C. Remarkably, the Au and Ni grains did not penetrate much further into the AlGaAs, and do still not reach the 2DEG. The most significant change with respect to Fig. 7.2c is that Au is diffusing underneath the Ni grains, reducing the total Ni–AlGaAs interface area. The results of Kuan *et al.* [5] indicate that this process is mainly responsible for the increase in contact resistance when a sample is being over annealed.

Kuan *et al.* [5] report that the contact resistance is sensitive to the ratio of the total contact area between Au regions and AlGaAs, and that of Ni regions. The Au–AlGaAs interface is considered a region of poor conductance because the Au grains (in contrast to Ni grains) do not contain any Ge, such that it cannot act as a source for diffusion of Ge into the heterostructure. However, it is to our knowledge not yet understood why the diffusion of Au underneath the Ni grains at later stages of annealing (when a large amount of Ge already diffused out of Ni) results in a strong increase of the contact resistance.

7.5 Diffusion model

Our qualitative picture of the formation of an ohmic contact is then as follows. In the initial stages of the diffusion process Au and Ge separate, and most Ge forms a new phase with the Ni. At the same time, these Ge-rich Ni grains move to the wafer surface due to a wetting effect, which results in the situation that the wafer surface is covered with neighboring Au and Ni grains. Next, both the Au and Ni grains penetrate into the heterostructure, which is compensated by a back flow of As and Ga into the Au and Ni grains. Meanwhile, Ge diffuses out of the Ni grains into the AlGaAs layer, and a good ohmic contact is formed when the AlGaAs layers are sufficiently doped with Ge al the way up to the 2DEG. In between the metal-rich phases and the 2DEG also some diffused Ni and Au can be found. At the same time Au is diffusing underneath the Ni grains, which have the lowest contact resistance with the doped AlGaAs layer. This increases the interface resistance between the metallization on the surface and the doped AlGaAs layer. Thus, the formation of an optimal contact is a competition between these two processes.

We use the above description to construct a model that predicts the optimal annealing time for a given annealing temperature and 2DEG depth d. The contact resistance is then the series resistance of the resistance of the Ge-doped AlGaAs region (R_{Ge}) and the interface resistance between the surface metallization and

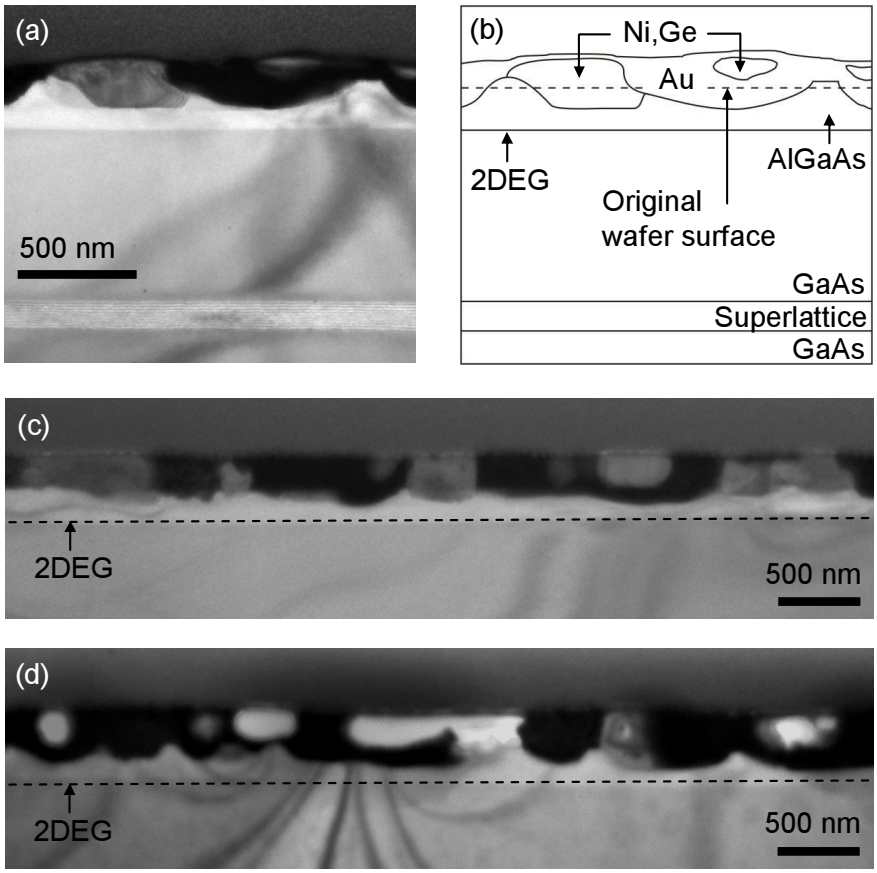

Figure 7.2: **(a)** Cross-section TEM image of a contact on wafer C, annealed for the optimal annealing time at 450 °C. **(b)** A sketch of the TEM image in **(a)** to specify the various layers and phases. **(c)** Larger area TEM image of the same contact as in **(a)** showing large Au (black) and Ni grains (dark gray) contacting the AlGaAs. **(d)** Similar image for a highly over annealed contact. The Au and Ni grains still do not penetrate the 2DEG, but Au has diffused underneath the Ni grains, which increases the contact resistance.

this Ge-doped AlGaAs layer (R_{if}). We will first assume an anneal temperature T that is constant in time. We model the resistance of the Ge-doped AlGaAs region using the result from work on n-GaAs that the contact resistance is inversely proportional to the doping concentration [8]. Thus, we assume that

$$R_{Ge} \propto \int \frac{1}{C(x)/C_0} dx, \tag{7.3}$$

where $C(x)/C_0$ is the local Ge concentration at depth x as in Eq. 7.1, and where the integral runs from the depth of the Au and Ni grains to the depth of the

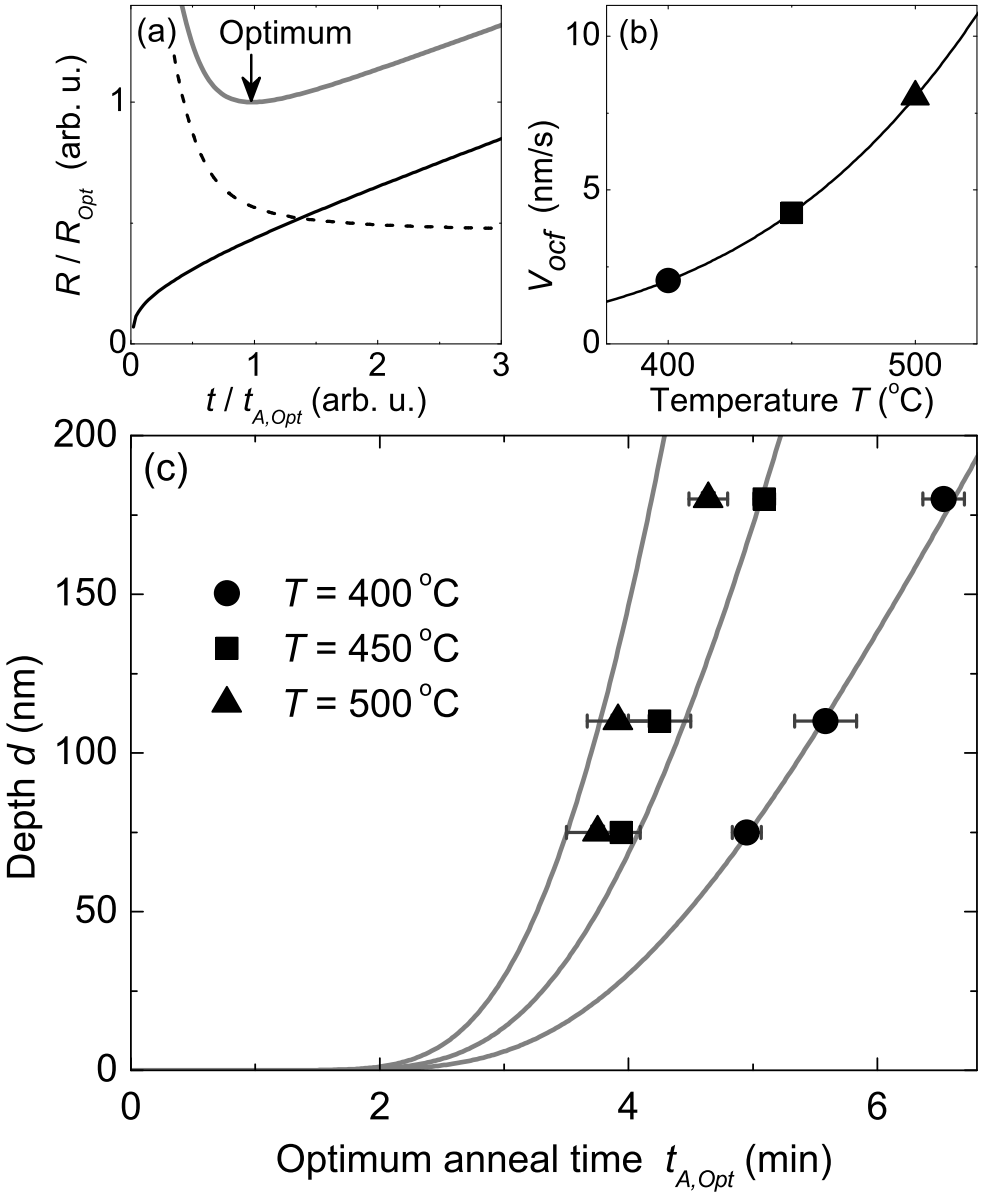

Figure 7.3: **(a)** Model for the resistance of an ohmic contact as a function of annealing time at constant temperature. The resistance R_{Ge} of the AlGaAs layers (dashed line) decreases in time due to increased Ge doping. The interface resistance R_{if} between the surface metallization and the Ge-doped AlGaAs layers (solid black line) increases in time due to a decreasing Ni–AlGaAs interface area. The time where the sum of these two resistances (gray solid line) shows a minimum defines the optimum annealing time $t_{A,Opt}$. **(b)** Effective velocity of optimal contact formation v_{ocf} as a function of temperature (Eq. 7.6), plotted for parameters that give the best fit in **(c)**. **(c)** Change in optimal annealing time as the 2DEG depth is (same experimental data as in Fig. 7.3. The solid gray lines (left to right for 500, 450 and 400 °C) represent fits using the model of Eqs. 7.5 and 7.6 (see text for details).

2DEG. The behavior of this equation is that R_{Ge} first rapidly decreases, and then curves off to saturate at a level that is proportional to d (dashed curve in Fig. 7.3a).

To model R_{if}, we assume that the increase in resistance for over annealed contacts is related to the decrease in Ni–AlGaAs interface area. Imagine, for simplicity, a single, square shaped Ni grain with area $A_{Ni} = L_{Ni}^2$. We model the reduction of this area as a sideways diffusion process of Au, again with a time-dependence as simple diffusion analogues to Eq. 7.1. The length of a side is then reduced as $L_{Ni}(t) \sim L_0 - 2\sqrt{4D_{Au}t}$, where L_0 is the initial grain size, and D_{Au} the diffusion constant for this process, such that

$$R_{if} \propto \frac{1}{(L_0 - 2\sqrt{4D_{Au}t}\,)^2}. \tag{7.4}$$

For a very wide parameter range, this model gives that R_{if} increases more or less linearly in time (solid black curve in Fig. 7.3a). A resistance increase that is much stronger than linear only sets in when the total interface area approaches zero, when the contact is already strongly over annealed. The total contact resistance is the sum of R_{Ge} and R_{if} (gray solid curve Fig. 7.3a), and the optimal annealing time is then defined as the time where this sum shows a minimum value.

We can reduce the number of fitting parameters for this modeling to only two with the following approach. For R_{Ge} in Eq. 7.3, we assume parameters where R_{Ge} saturates at a value below, but on the order of the optimal contact resistance R_{opt}. We also assume that this saturation occurs in a time scale on the order of a few times the optimal annealing time. For R_{if} in Eq. 7.4, we assume that it has a value below R_{opt} for $t = 0$, and that it increases more or less in a linear fashion to a value of order R_{opt}. This increase should take place in a time scale on the order of the optimal annealing time. Numerically investigating this model then shows that it has for a very wide parameter range the behavior that the increase of optimal annealing time $t_{A,Opt}$ with increasing 2DEG depth d is close to linear. We can express this using an effective velocity for optimal contact formation v_{ocf},

$$t_{A,Opt} = d/v_{ocf}. \tag{7.5}$$

Furthermore, numerical investigation of the temperature dependence shows that v_{ocf} behaves according to

$$v_{ocf}(T) = v_0\ exp(-\frac{E_a}{k_B T}) \tag{7.6}$$

when the diffusion processes that underlie Eq. 7.3 and Eq. 7.4 are both thermally activated with a similar activation energy E_a. We can now fit this model to our

experimental data only using Eq. 7.5 and Eq. 7.6, such that we only have v_0 and E_a as fitting parameters. In doing so, we take again into account that the temperature $T(t)$ is not constant during annealing, and use again profiles as in Fig 7.1a.

The results of this fitting are presented in Fig. 7.3c, and v_{ocf} as a function of temperature for these fitting parameters ($E_a = 0.6$ eV and $v_0 = 7.6 \cdot 10^{-5}$ m/s) is plotted in Fig. 7.3b. While it is a crude model, the fits are very reasonable, showing that the model is useful for predicting optimal annealing times. Furthermore, the value for E_a is a realistic number [7]. Our model also predicts that the minimum value of the resistance that can be achieved for optimally annealed contacts increases with increasing 2DEG depth. We did not observe such a clear trend, probably because the resistance of optimal contacts is so low that one needs to include contributions from 2DEG square resistance around and underneath the contact when evaluating absolute values (further discussed below).

Our model for the annealing mechanism implies that optimal contacts have a rather uniform Ge concentration throughout the AlGaAs layers, which results in a value for R_{Ge} of about 10 Ω. This implies that the bulk resistivity in the doped Ge-doped AlGaAs layer is around 4 Ωm. In turn, this implies that in-plane electron transport under an optimal contact from the metallization on the surface to 2DEG on the side of the contact still mainly takes place in the original 2DEG layer. If the square resistance $R_\square$ for transport in the the original 2DEG layer does not strongly increase during annealing ($R_\square$ for 2DEG before annealing is typically 5 Ω), this also implies that the resistance of optimal contacts should be inversely proportional to the contact area. Thus, measuring whether the contact resistance depends on contact area or on the circumference of a contact can give further insight in the annealing mechanism.

We carried out such a study, by varying the shape of contacts. All results that we discussed up to here were obtained with square contacts with an area A of 0.04 mm^2 and a circumference $C_L = 4L$ of 0.8 mm. For the dependence on contact shape, we measured various sets where we varied the circumference C_L while keeping the area constant at 0.04 mm^2, and various sets where we varied the area while keeping the circumference constant at 0.8 mm. We varied the shape from smooth circular shape to square shapes with a zig-zag edge at the 50 micronscale, to avoid getting too much resistance contribution from square resistance of 2DEG right next to a contact (for these devices we used electron-beam lithography). All contacts were fabricated and annealed in one single batch to ensure that it is meaningful to compare the values of contact resistance.

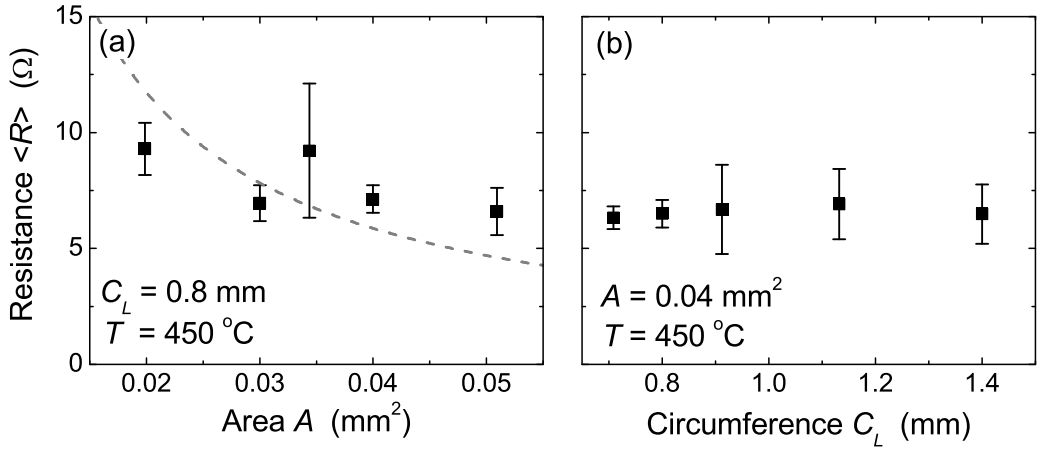

Figure 7.4: Contact resistance $\langle R \rangle$ as a function of **(a)** contact area A for constant circumference $4L$ and **(b)** contact circumference C for constant area A. The error bars here represent the standard deviation from measuring R on 8 identical contacts. The dashed line in **(a)** is a fit using $\langle R \rangle \propto 1/A$.

On contacts that are not annealed, we can observe a tunnel current, as expected for Schottky barriers. Here, the effective resistance is inversely proportional to area. For optimally annealed contacts on wafer A, we found that the contact resistance was independent on circumference, while only showing a very weak dependence on area (much weaker than inversely proportional to area), see Fig. 7.4. The fact that the dependence on shape does here not show a clear dependence as $\langle R \rangle \propto 1/A$ agrees with the fact that the $\langle R \rangle$ values are comparable to the square resistance of the 2DEG, such that the latter gives a significant contribution to the total contact resistance. Fully understanding the contact resistance then requires incorporating all square resistance contributions from underneath and around the 2DEG. Since we found it impossible to estimate these effects with a small error bar, we turned to measuring under annealed contacts instead.

On two sets of under annealed contacts on wafer A, where we used a different anneal time t_A (average contact resistance of 30 Ω and 500 Ω), we found (within error bar) no dependence on area or circumference. We can only explain this result if we assume that the 2DEG square resistance underneath the contact is significantly increased (to values comparable to the total observed contact resistance) for under annealed contacts. This probably results from the in-diffusing Ge, which already introduces strain and scatter centers in the 2DEG layer before optimal contact conditions are reached. For optimal annealed contacts (here with total resistance of typically 7 Ω, independent of circumference), the square

resistance underneath a contact must have returned to a value of less than 10 Ω. Apparently, the resistance increase due to strain and scatter centers is overcompensated by increased Ge doping near the 2DEG layer.

The summary of this study is that we never obtain a clear dependence on circumference, and only a weak dependence on area for optimal contacts. We can, nevertheless, draw the following conclusions. For an optimal ohmic contact, it is *not* the case that electron transport between the surface metallization and the surrounding 2DEG mainly occurs at the edge of a contact. Instead, the full contact area plays a role, and in-plane electron transport under an optimal contact mainly takes place in the original plane of the 2DEG. In addition, we find it impossible to evaluate the absolute values of the contact resistance of our devices with an accuracy within a factor 2, since the resistance of an optimal contact has a contribution from the square resistance underneath the contact, and its value is influenced by the annealing process. We can therefore not study the property of our model that the optimal contact resistance value should be proportional to d. Instead, we should evaluate whether the enhanced square resistance underneath a contact needs to be incorporated in our model. We find that this is not needed for the following reasons: for over annealing it does not play a role, since we observe the same over-annealing mechanism as observed on bulk n-GaAs. Optimally annealed contacts occur when the square resistance underneath the contacts has again values well below 10 Ω. Here we observe a weak area dependence and no dependence on circumference, such that we can rule out that the effect dominates the contact resistance here. Thus, the only effect is that it temporarily enhances the total contact resistance by about a factor 2 while the annealing progresses towards optimal contact conditions. Note that it does not change the fact that lowering the contact resistance in this phase still fully depends on further Ge diffusion towards the 2DEG layer. Therefore, it only slightly modifies how R_{Ge} in Eq. 7.3 decreases towards low values.

7.6 Conclusions

Summarizing, we have measured the zero-bias resistance of annealed AuGe/Ni/Au contacts to a 2DEG as a function of annealing time and temperature. We have thus obtained optimal annealing parameters for three different heterostructures where the 2DEG lies at a different depth with respect to the surface of the wafer. TEM images of several annealed contacts provided further insight into the annealing mechanism and the formation of a good ohmic contact. Combining this

information we have developed a model that can predict the optimal annealing parameters for contacting a 2DEG at a certain depth in a GaAs/AlGaAs heterostructure. This model should have predictive value for many heterostructures, as long the temperature of the samples as a function of time during the annealing process is known. Our model may become invalid for systems with a very deep 2DEG, since R_{if} (Eq. 7.4) is expected to increase more rapidly at long annealing times, possibly resulting in non-ohmic behavior. Our model suggests that for solving this problem the focus should be at maintaining sufficient contact area between Ni grains and the Ge-doped AlGaAs layer at long annealing times. This can possibly be engineered by changing the layer thickness, order and composition of the initial AuGe/Ni/Au metallization.

We thank B. H. J. Wolfs, M. Sladkov and S. J. van der Molen for help and valuable discussions, and the Dutch Foundation for Fundamental Research on Matter (FOM) and the Netherlands Organization for Scientific Research (NWO) for funding.

References

[1] See for example C. W. J. Beenakker, H. van Houten, Solid State Physics **44**, 1 (1991).

[2] For a review see A. G. Bacas *et al.*, Thin Solid Films **308-309**, 599 (1997).

[3] N. Braslau, J. B. Gunn, J. L. Staples, Solid State Electronics **10**, 381 (1967).

[4] M. Ogawa, J. Appl. Phys. **51**, 406 (1980).

[5] T. S. Kuan *et al.*, J. Appl. Phys. **54**, 6952 (1983).

[6] A. K. Kulkarni, and C. Lai, J. Vac. Sci. Technology A **6**, 1531 (1987).

[7] A. K. Kulkarni, and C. Lai, Thin Solid Films **164**, 435 (1988).

[8] N. Braslau, J. Vac. Sci. Technology **19**, 803 (1981).

[9] N. Braslau, Thin Solid Films **104**, 391 (1983).

[10] R. P. Taylor *et al.*, J. Appl. Phys. **76**, 7966 (1994).

[11] R. P. Taylor *et al.*, Superlattices and Microstructures **24**, 337 (1998).

[12] G. Sai Saravanan *et al.*, Semicond. Sci. Technol. **23**, 025019 (2008).

[13] H. H. Berger, Solid State Electronics **15**, 145 (1972).